Density functional theory investigation of the geometric and spintronic structure of *h*-BN/Ni(111) in view of photoemission and STM experiments

G. B. Grad, P. Blaha, and K. Schwarz
Technical University of Vienna, Getreidemarkt 9/165, A-1060 Vienna, Austria

W. Auwärter and T. Greber
Physics Institute of the University of Zürich, Winterthurerstrasse 190, CH-8057 Zürich, Switzerland

The (1×1) commensurate layer of hexagonal boron nitride on nickel is investigated by density functional theory calculations. The full-potential linear-augmented-plane-wave method is used to obtain total energies for different structural models, the spin-resolved band structure, and local density of states (LDOS) above the surface. The calculations confirm the accepted structure model of a corrugated layer with nitrogen placed at on-top sites. From the remaining two possibilities for boron the one with boron on fcc hollow sites is energetically slightly favored, but the energy difference to the structure with boron on the hcp hollow site is smaller than the thermal energy during *h*-BN synthesis. The spin-resolved electronic (spintronic) band structure indicates *h*-BN to be an insulator. The calculated band structure of the π and σ bands agrees well with photoemission data. The polarization-induced charge transfer from *h*-BN to Ni reduces the magnetic moment in the Ni top layer below the bulk value. The LDOS in front of the surface indicates distinct atomic sites in scanning tunneling microscopy (STM) images which are complemented with STM images. From the distance dependence of the LDOS for Ni(111) and *h*-BN/Ni(111) the apparent height of heteronuclear atomic steps may be derived. From its spin and energy dependence we propose tunneling experiments with strong magnetic contrast.

I. INTRODUCTION

Hexagonal boron nitride is an insulating material, isostructural to semimetallic graphite. Much attention has been paid to *h*-BN in relation to its technological applications. On Ni(111) it forms an atomically sharp, almost perfect overlayer. *h*-BN/Ni(111) is thus a prototype system for the study of magnetic metal insulator interfaces. The *h*-BN layer is only weakly bound to the substrate but remains stable up to over 1000 K. A recent experimental investigation showed, e.g., that the very low surface energy of *h*-BN leads to a strongly temperature-dependent sticking coefficient for cobalt and to Co intercalation at elevated temperatures.[2] (1×1) commensurate single atomic layers of *h*-BN may be grown[3] using the reaction of borazine $[(BNH)_3]$ with Ni(111) at 1000 K. Experimental structure determinations by two independent groups indicated single-domain *h*-BN/Ni(111) which shows the importance of the second Ni layer in the formation process of the structure.[1,4,5] Here, the geometric structure of *h*-BN/Ni(111) is investigated for the observed equilibrium structure and five other high-symmetry structures. Scanning tunneling microscopy (STM) images show a hexagonal Bravais lattice with a two-atom base that forms a honeycomb pattern. This corresponds to a well-ordered surface with two distinct atomic species, but it was not possible to make a clear assignment of the two atomic species and sites.[1] The theoretical local densities of states (LDOS) above the surface are correlated with the Tersoff-Haman formula[6] to experimental STM data. The LDOS dependence on the electron energy relative to the Fermi level is studied for the two spin directions and an STM experiment with maximum magnetic contrast is proposed.

II. THEORETICAL METHOD

Self-consistent calculations of total energies and the electronic structure based on the scalar relativistic full-potential (FP) ''augmented-plane-wave+local orbitals'' method (APW+lo) (Refs. 7 and 8) were carried out using the WIEN2k code.[9,10] This is a very accurate and efficient scheme to solve the Kohn-Sham equations of density functional theory (DFT) in which exchange and correlation effects are treated, for example, by the generalized gradient approximation (GGA) which often leads to better energetics and equilibrium structures than the local density approximation (LDA).[11] The electron density is obtained by summing over all occupied Kohn-Sham orbitals and plays the key role in this formalism. Besides the ''linearizing'' local orbitals for *s*, *p*, and *d* valence states of the standard APW+lo basis additional LO's are added in order to describe the 3*p* (semicore) states of Ni and the 2*s* in N. The atomic sphere radii were 2.0 a.u. for Ni and 1.35 for both B and N. The required precision in total energy was achieved by using a large plane-wave (PW) cutoff. In the linear APW (LAPW) method the relevant convergence parameter is RK_{max}, which is defined by the product of the smallest atomic sphere radius times the largest reciprocal lattice vector of the PW basis. We use $RK_{max} = 7.5$ for Ni(111) and $RK_{max} = 6.0$ for *h*-BN/Ni(111). This corresponds to an energy cutoff of 14 Ry and 19.8 Ry, respectively. A *k*-point sampling of up to 4000 points in the full two-dimensional (2D) Brillouin zone (BZ) was used. The *k* mesh is generated in the irreducible wedge of the Brillouin zone on a special point grid which can be used in a modified tetrahedron scheme.[12]

The Ni(111) and *h*-BN/Ni(111) surfaces were modeled by

periodic slab supercells with a vacuum region of 20 Bohrs. The geometry optimization was first performed using 7 Ni layers, which was found to be sufficient for this purpose. All other results were produced using this optimized geometry for the surface layers, but adding additional bulk layers forming a much thicker slab of 19 layers of Ni. Such large slabs are necessary to reduce the spurious surface-surface interactions, which otherwise lead to a splitting of the two surface states.[13] Preliminary calculations with a smaller vacuum or using only 7 Ni layers have shown that the two surfaces interact weakly with each other via the "bulk" as well as via the "vacuum," producing a spurious splitting of the surface states into a "bonding" and "antibonding" state. This splitting vanishes by using the large slab.

III. EXPERIMENTS

The photoemission experiments were performed in a modified VG ESCALAB 220 spectrometer with monochromatized He Iα radiation.[14] The overall energy-momentum resolution was better than 50 meV/0.02 Å^{-1} full width at half maximum (FWHM) and the presented data were taken at room temperature. The preparation of the h-BN layers and the Ni(111) substrate is described elsewhere.[1,3] The presented scanning tunneling microscopy data were taken from Ref. 1.

IV. GEOMETRIC STRUCTURE

Single-layer h-BN grows epitaxially on Ni(111) as found by several experiments.[1,4,5,15–17] The positions of B and N with respect to the Ni-surface sites and their height above the Ni surface are known from different experiments. The electron diffraction indicated single-domain h-BN.[1,4] Nevertheless, STM from incomplete layers find sometimes different orientations of islands, leading to speculations about different orientations of h-BN with respect to the Ni(111) substrate.

Three high-symmetry sites are possible for B and N above the hexagonal Ni(111) surface: namely, *top*, *fcc*, and *hcp* sites. We label these six possible configurations by their N and B positions (see Fig. 1). In a close-packed layer system the fcc site is occupied in every third layer (ABCABC . . .), while the hcp site is occupied in every second layer (ABAB . . .).

We have performed total energy calculations for the six possible configurations that can be formed by the monolayer h-BN/Ni(111) exhibiting a 1×1 structure, shown in Fig. 1. Structure relaxation was done using the forces acting on the atoms to move them to their equilibrium positions so that we can compare the total energies of the six configurations corresponding to their minimum energy. It turns out that only for two configurations is h-BN bound at all to the Ni surface—namely, when the N atoms are on top of the topmost Ni atoms—whereas for all other configurations the h-BN layer is unbound. Thus it seems to be essential that the N atom sits directly on top of a Ni atom. For this on-top position two possibilities remain for the B atom: namely, to occupy the fcc or the hcp hollow site, respectively. We find

(N,B)=(top,fcc)　　(N,B)=(hcp,top)　　(N,B)=(fcc,hcp)

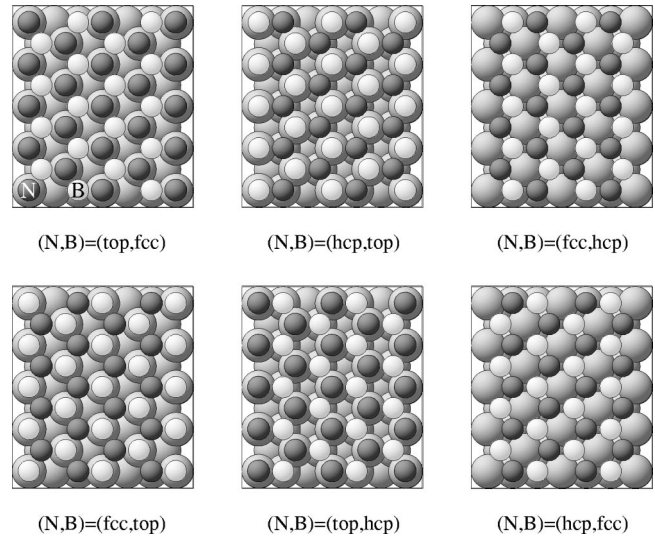(N,B)=(fcc,top)　　(N,B)=(top,hcp)　　(N,B)=(hcp,fcc)

FIG. 1. Possible (1×1) configurations for one-monolayer h-BN/Ni(111). The *top*, *fcc* hollow, and *hcp* hollow sites are considered for the position of the nitrogen and boron atoms, respectively.

that the fcc hollow site, denoted as (N,B)=(top,fcc), is energetically the most favorable. In Fig. 2 we show the distances in the z direction between the Ni layers and the h-BN surface with respect to the top Ni layer for the ground-state configuration. The h-BN layer is buckled by about 0.1 Å with the B atom closer to the Ni surface than N. The agreement with the experimental results[4,5] is very good, considering that the GGA underestimates the bonding and tends to
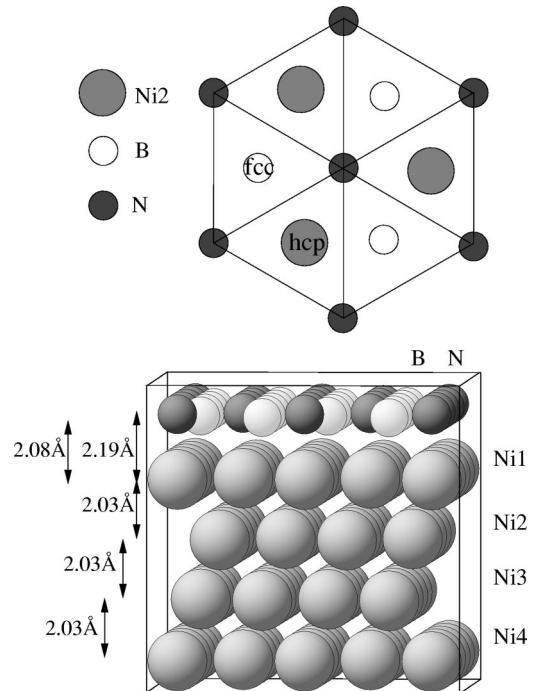

FIG. 2. Structure parameters of the minimum energy configuration (N,B)=(top,fcc). For nitrogen an outward corrugation of 0.1 Å is found.

obtain equilibrium distances larger than the LDA and sometimes than experiment. The energy difference between (N,B)=(top,fcc) and (top,hcp) is 18 ± 4 meV (Ref. 18) per unit cell (which contains two h-BN surfaces separated by the vacuum). This very small value may be understood since differences between (top,fcc) and (top,hcp) are only related to the second (and deeper) Ni layers that are expected to make a much smaller contribution to the bonding. The energy difference is also much smaller than $k_B T_s$, where T_s = 1000 K is the temperature of the h-BN/Ni(111) synthesis. This indicates that kinetic effects must be important for the dominance of the (top,fcc) phase. The present GGA calculation might not have the accuracy to decide conclusively between these two structures.

V. ELECTRONIC STRUCTURE

Hexagonal boron nitride is isoelectronic to graphite. It has covalent sp^2 bonds that form the hexagonal network of individual layers. In contrast to graphite the heteronuclear BN base imposes ionicity and drives h-BN to be insulating with a band gap of ≈ 5 eV.[19]

For the case of a single layer of h-BN on Ni(111) one would not expect a strong influence of this insulator on the electronic (and spintronic) structure of the underlying metal since at the Fermi energy no BN states are available for hybridization with the substrate. However, the h-BN layer gets polarized upon adsorption on a metal and charge transfer (or displacements) may occur which would decrease the work function. This charge transfer does not imply hole doping of h-BN since the displaced charge remains localized in the interface. It does, however, reduce the spin magnetic moment of the Ni top layers[20] (see below). The fact that tunneling microscopy may be performed on h-BN/Ni(111) (Ref. 1) does, on the other hand, indicate "metallicity" in the sense that electrons may tunnel across a vacuum/h-BN/Ni(111) interface. In Fig. 3(a) an experimental photoemission dispersion plot from h-BN/Ni(111) is shown along the $\bar{\Gamma}\bar{K}$ direction. The σ and π bands are clearly resolved and nicely follow the calculated band structure. The experimental π band width of 5.5 eV matches the spin-averaged theoretical width (5.52 eV) and is in fair agreement with the photoemission experiment of Nagashima *et al.* (5.8 eV).[15] The experimental $\sigma(\bar{\Gamma})-\pi(\bar{K})$ energy difference is 0.8 eV and agrees as well with Nagashima *et al.* (0.9 eV),[15] while the theoretical energy difference is spin dependent, 0.04 (0.29) eV for spin up (down), respectively, and significantly smaller than the experimentally observed energy difference. This suggests that the two bands with different character relax differently upon the creation of a hole in the photoemission process where the self-energy of the σ band appears to be larger than that of the π band.

In Fig. 3 the band structure of the slab containing 19 layers of Ni+2 layers of corrugated h-BN is shown for the two high-symmetry directions in the two-dimensional hexagonal Brillouin zone for spin-up and spin-down electrons, respectively. The magnetism is reflected in the flat, exchange-split Ni d bands which are partially empty for minority spins. In order to identify the h-BN-related bands they
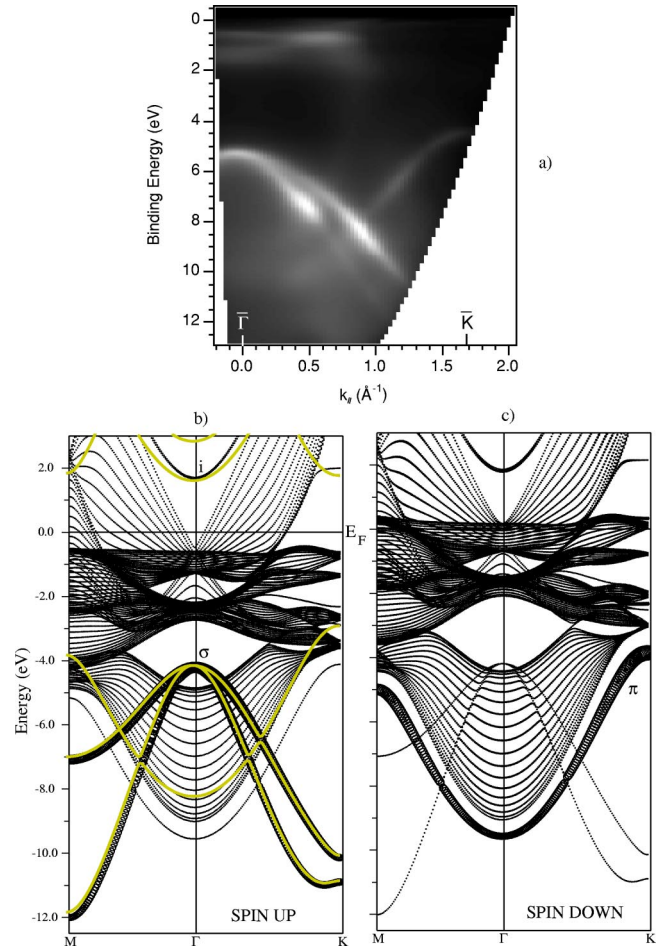

FIG. 3. Top: (a) Experimental gray scale dispersion plot on the $\bar{\Gamma}$-$\bar{K}$ azimuth as extracted from angular-resolved He Iα photoemission data. The gray scale reproduces the intensity (white = maximum) and $k_\parallel$ is determined by $\sin(\theta)\sqrt{2m_e E_{kin}}/\hbar$, where θ is the polar emission angle. Bottom: the theoretical band structure of h-BN/Ni(111) in the $\bar{M}$-$\bar{\Gamma}$-$\bar{K}$ directions in the hexagonal reciprocal unit cell. (b) Spin up, the radius of the circles is proportional to the partial p_x+p_y charge density centered on the nitrogen sites (σ bands); we include by thick yellow lines the bands of a buckled freestanding h-BN monolayer, which have been aligned at the N-σ band at Γ. (c) Spin down, the radius of the circles is proportional to the partial p_z charge density on the nitrogen sites (π bands).

were projected on atomic orbitals centered on the nitrogen site. In Fig. 3(b) (majority spin) the weights of the in-plane p_x+p_y (sp^2) orbitals are shown with circles of corresponding size. These states form the σ bands which are degenerate at $\bar{\Gamma}$. In Fig. 3(c) (minority spin) the weights of the p_z orbitals (π bands) are shown. The π band lies below the Ni d band, and neither crosses the Ni sp band nor contributes to the conductivity. The first h-BN-derived conduction band is found above the Fermi level. It has positive effective mass and is centered at $\bar{\Gamma}$. For bulk h-BN Catellani *et al.* found such bands as well, which they identified as an interlayer band.[19] In our case the main weight lies in the topmost Ni layer and we term this band interface-state band [labeled with "i" in Fig. 3(b)]. In Fig. 3(b) we plot with a colored

TABLE I. Band parameters (E_F-E) (eV) from h-BN/Ni(111), flat and buckled single h-BN layers at $\bar{\Gamma}$ and $\bar{K}$. For the single layers no exchange splitting occurs and the energies have been adjusted arbitrarily to $\sigma_{\uparrow}(\bar{\Gamma})$ of h-BN/Ni(111).

	π band		σ_1 band		σ_2 band		Interface
	$\bar{\Gamma}$	$\bar{K}$	$\bar{\Gamma}$	$\bar{K}$	$\bar{\Gamma}$	$\bar{K}$	$\bar{\Gamma}$
Experiment	10.0	4.5	5.3	-	5.3	-	-
Theory ↑	9.60	4.21	4.25	10.99	4.25	10.23	−1.63
Theory ↓	9.61	3.95	4.23	10.99	4.23	10.24	−1.75
BN-flat	8.26	2.93	4.25	10.94	4.25	10.12	−1.76
BN-buckled	8.33	3.02	4.25	10.95	4.25	10.17	−1.50

(yellow) line the bands corresponding to a calculation of a single freestanding corrugated h-BN layer. In Fig. 3(b) and Table I the energies of the σ band at $\bar{\Gamma}$ have been adjusted to the values from the h-BN/Ni(111) slab. From this we see that the σ-type bands and π band do not show much difference compared to their corresponding bands with the Ni substrate. However, the relative shift between the σ bands and the π bands is about 1.3 eV, indicating a strongly different interaction of the two band types with the substrate. In particular the nominal gap increases from 4.5 eV for the bare, buckled layer to 5.8 eV for the buckled layer on Ni(111). The buckling or corrugation of the h-BN only weakly affects the electronic structure: i.e., the gap increases by 0.2 eV in going from the corrugated to the flat h-BN with the same surface unit cell. This indicates that h-BN makes no significant contribution to bands that cross the Fermi level, and it is thus considered to be an insulator.

It is remarkable that the energies of the h-BN π band depend on the spin of the electrons. It does, however not imply magnetic h-BN since none of the exchange-split bands crosses the Fermi level. The substrate-induced exchange splitting decreases with the distance in energy from the Ni d band—i.e., is largest (≈ 260 meV) for the π band at $\bar{K}$ (see Table I). The unoccupied interface state appears as well to be exchange split by ≈ 130 meV. We expect that an experiment with a spin analysis should resolve these exchange splittings, which are smaller than the intrinsic linewidth in photoemission. In Table I calculated and observed band parameters of h-BN are listed for the π, σ, and interface-state bands of h-BN on Ni(111). The last two rows correspond to the calculated freestanding h-BN monolayer. Flat BN refers to B and N atoms in the same plane and BN buckled to the h-BN layer with the corrugation of h-BN/Ni(111).

The σ bands at the $\bar{K}$ point may not be resolved by He Iα photoemission because the accessible $k_\parallel$ range at this photoelectron energy is too small [see Fig. 3(a)].

The experimental work function shifts by 1.8 eV from 5.3 eV to 3.5 eV in going from Ni(111) to h-BN/Ni(111).[15,20] This indicates that the h-BN layer gets polarized by the nickel substrate. The calculations for a single (freestanding) layer of h-BN with the experimental corrugation,[1] but without substrate, indicate a charge transfer of 0.56 electrons from boron to nitrogen. This charge transfer is due to the higher electronegativity of nitrogen and makes h-BN an in-
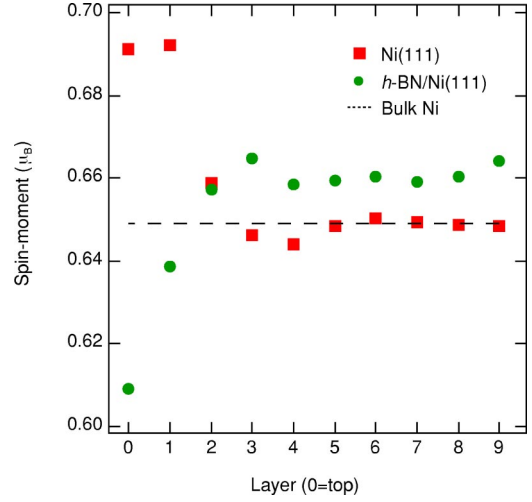

FIG. 4. Calculated layer dependence of the spin magnetic moments in the first 10 layers of a 19-layer slab for Ni(111) and h-BN/Ni(111) [0 is the top (surface/interface) Ni layer]. The dashed line is the result of a 3D Ni calculation without surface. The surface magnetic moment of nickel is reduced by the h-BN layer.

sulator. The charge on the atoms was determined with Bader's "atoms-in-molecules" method (AIM).[21] In the case of h-BN/Ni(111) the AIM procedure yields a charge of 0.59 electrons on nitrogen and -0.65 electrons on boron. Therefore the net charge transfer to the substrate is 0.06 electrons per unit cell and the ionicity of the BN bonds even increases as does the gap. Within an electrostatic picture, where a charge separation length of ≈ 1 Å is assumed, this yields a work function shift of 2 eV that has the sign and the same order of magnitude as the experimental observation. The calculated electrostatic potentials $(V-E_F)$, 0.5 nm away from the top layer, are 5.1 and 3.4 eV for Ni(111) and h-BN/Ni(111), respectively. This results in a calculated work function shift of 1.7 eV which is in good agreement with experiment.

In Fig. 4 the layer-resolved magnetic moments are shown. The charges in the individual spin channels have been determined inside the atomic spheres in the individual Ni layers of the slab. This figure shows only ten layers since the second half of the slab is redundant due to symmetry reasons. For Ni(111) we find a slightly higher bulk magnetic moment ($0.66\mu_B$) than in a previous LDA study of Fu and Freeman[22] ($0.58\mu_B$) and the surface enhancement of the magnetic moment is 6% only. However, the trend is identical; in particular the two topmost layers have similar high magnetic moments before they decrease to the bulk value.[22,23] Furthermore, the calculations do indicate Friedel-type oscillations of the magnetic moment with an amplitude of less than 0.5% and a wavelength in the order of three to four layer spacings. In the case of h-BN/Ni(111) the magnetic moment in the top Ni layer appears to be reduced by $0.08\mu_B$ with respect to the pure Ni(111) top layer.[24] Interestingly, the Friedel-type oscillations of Ni(111) and h-BN/Ni(111) are not exactly in phase and even a 19-layer slab does not yield full convergence to the bulk value ($0.65\mu_B$). [Note that the number of layers in the surface supercell calculation fixes

indirectly a particular k mesh in the k_z direction.] The reduction of the bulk magnetic moment can be explained in terms of charge transfer from BN to Ni, and since around the Fermi level mainly Ni minority d-band states are available, this charge transfer dopes the unoccupied minority d-band states and reduces the magnetic moment. This reduction mechanism of the magnetic moment due to charge transfer has thus a different quality than the hybridisation mechanism of Tersoff and Falicov.[23]

VI. INTERPRETATION OF STM DATA FROM h-BN/NI(111)

We combine the theory of Tersoff and Hamann for tunneling between a real surface and a model probe tip[6] with our *ab initio* calculations based on the FP-LAPW method and compare them to scanning tunneling microscopy experiments of Auwärter *et al.*[1]

Considering the tunneling current I_t given to first order by Bardeen's formalism,[25] Tersoff and Hamann[6] take the limit to small voltage and temperature,

$$I_t = \frac{2\pi e}{\hbar} \sum_{\nu,\mu} |M_{\mu,\nu}|^2 \delta(E_\mu - E_F)\delta(E_\nu - E_F), \qquad (1)$$

where E_μ and E_ν are the energies of the states in the tip and surface, respectively, and $M_{\mu,\nu}$ are the tunneling matrix elements. In the limit when the tip is replaced by a point probe, the tip wave functions are completely localized: then the matrix element is simply proportional to the density of states imposed by the substrate wave function ψ_ν at the position r_0 of the tip (probe) and simplifies to

$$I_t \propto \sum_\nu |\psi_\nu(r_0)|^2 \delta(E_\nu - E_F). \qquad (2)$$

For $E_\nu = E_F$ the tunneling current is the surface LDOS at E_F. Thus the tunneling current is proportional to the surface LDOS at the position of the point probe, and the microscope image represents a map of the LDOS above the surface.

In Fig. 5 the contour plots of the charge density for both the bare Ni surface and h-BN on Ni(111) are shown. The plots correspond to the spin-up+spin-down contributions at $E_F \pm 0.08$ eV taken at a distance of 2.5 Å from the surface. For both spins the trend is the same, so we only show the sum of both spin channels. In Fig. 5(a) we present the valence charge density of the bare Ni(111) surface in the plane parallel to the surface at 2.5 Å from the topmost Ni layer. The main contribution to the charge is on top of the topmost Ni atoms, less charge is in the fcc sites, and the minimum corresponds to the hcp hollow sites. The hcp and fcc sites are only slightly different in the LDOS map, which indicates the low importance of the second Ni layer—and that it is difficult to obtain Ni(111) substrate STM images that resolve a two atomic base. In Fig. 5(b) the valence charge density of h-BN/Ni(111) in the plane 2.5 Å above the N atoms is shown. The main contribution stems from on top of the N atoms but the fcc and hcp sites show a significant difference where tunneling from boron sites (fcc) is more likely than from the empty hcp sites.
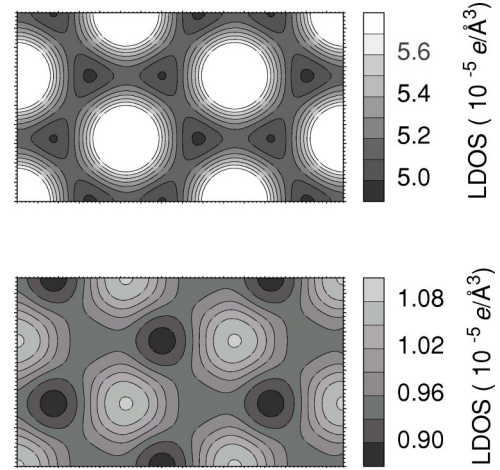

FIG. 5. Local charge density ± 0.08 eV around the Fermi level at a distance $r_0 = 2.5$ Å above the corresponding top layer for the bare Ni(111) (top panel) and the h-BN/Ni(111) surface (bottom panel). The units are in $e/Å^3$, illustrated by corresponding gray shadings.

Figure 6 shows a STM picture with atomic resolution as obtained by Auwärter *et al.*[1] of the surface after formation of a h-BN layer on Ni(111). It was recorded at constant height with a tungsten tip at+4.8 mV bias voltage. This experimental image presents a hexagonal Bravais lattice with a two-atom base that forms a honeycomb pattern. These findings stand for a well-ordered surface with two distinct atomic species and a dark spot in the center of the hexagon. The lattice constant of 2.5 ± 0.1 Å corresponds to that of the Ni(111) substrate. From a comparison with Fig. 5(b) the bright spots can be assigned to the nitrogen sites and the intermediate intensity spots to those of boron sites (fcc). The consistency of experiment and the Tersoff-Hamann picture tell us that for this case the tip wave function is compatible with the (assumed) s character of the tip wave function.[26]
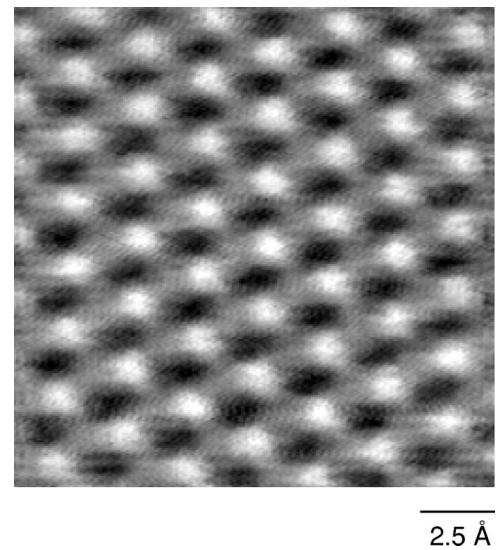

2.5 Å

FIG. 6. Atomically resolved STM image of h-BN/Ni(111) ($V_t = 4.8$ mV, $0.2 < I_t < 0.5$ nA) from Ref. 1. Note the vision of a hexagonal Bravais lattice with a two-atom base.
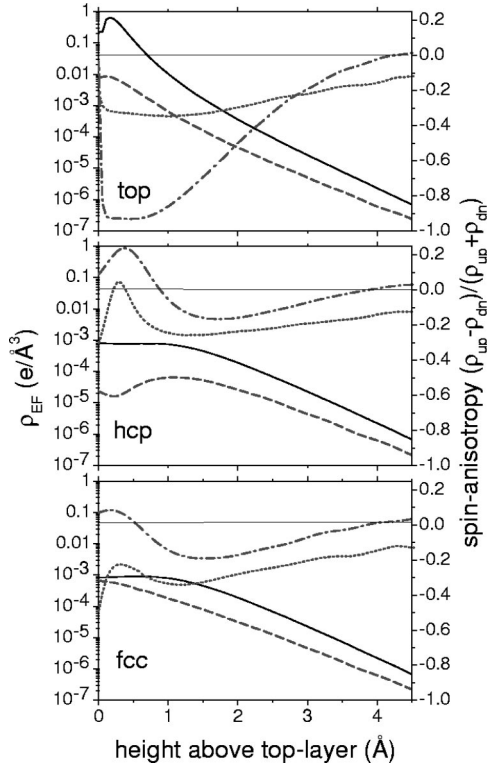
FIG. 7. Charge density ρ (± 0.08 eV around the Fermi level [solid lines, Ni(111); dashed lines, h-BN/Ni(111)] and corresponding spin anisotropy $(\rho_{up}-\rho_{down})/(\rho_{up}+\rho_{down})$ [dash-dotted lines, Ni(111); dotted lines, h-BN/Ni(111)] as a function of the height above the top layer for the three inequivalent high symmetry sites: *top*, *hcp*, and *fcc*.

In a further step we investigated the height (r_0) dependence of $|\Psi_\nu|^2(E_F)$ for both spin channels and for the three high-symmetry sites *top*, *fcc*, and *hcp* in the unit cell. Figure 7 shows the charge density at E_F for Ni(111) and h-BN/Ni(111) as a function of the height (r_0) above the top layer and the spin anisotropy $(\rho_{up}-\rho_{down})/(\rho_{up}+\rho_{down})$. For $r_0 < 1$ Å the electronic shell structure of the substrate becomes important, though this range is not accessible for STM experiments. For $r_0 > 1$ Å, both cases Ni(111) and h-BN/Ni(111) show an exponential charge density decrease with about the same decay length λ. From a comparison of these exponential slopes in Figs. 7(a)–7(c) it can be seen that in Fig. 5 no change in contrast is expected for different tunneling distances. However, at a given r_0 the electron density is larger for metallic Ni(111) than for h-BN/Ni(111). For a constant tunneling barrier this indicates that in a constant-conductance STM picture, where the topography is shown, the Ni-Ni steps are expected to be mapped with a higher contrast (height) than the Ni–h-BN steps although the true height of both step types is about the same. Homonuclear steps show their true height z_0 in a topograph. In heteronuclear steps, e.g., a step between Ni and a h-BN island, the height seen in the topograph is modified by the ratio α of the LDOS and the different tunneling barriers. $\alpha(E-E_F, r_0)$ is the ratio between the local DOS of Ni(111), $|\Psi_{Ni}|^2$, and that of h-BN/Ni(111), $|\Psi_{h-BN}|^2$, at a height r_0 above the surface. Assuming the same tunneling barriers below and above a
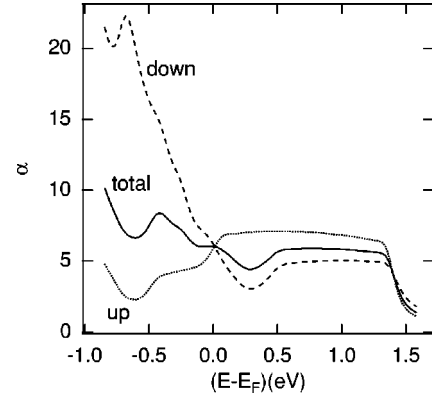

FIG. 8. Energy and spin dependence of α, the ratio of the local densities of states of Ni(111) and h-BN/Ni(111) at a distance of 5 a.u. from the top layer. The densities are averaged over the surface unit cell.

heteronuclear step, we get for the apparent height $r_0 = z_0 - \Delta z$, an electronic contrast Δz given by α and λ, i.e., $\Delta z = \lambda \ln \alpha$, where λ is the exponential decay length of the charge density $|\Psi_\nu|^2 \propto \exp{-r_0/\lambda}$ (see Fig. 7). It can furthermore be seen that it is more likely for electrons to tunnel across h-BN than a corresponding vacuum layer and the tunneling has an other spin dependence than in the vacuum. In particular the spin anisotropy for h-BN/Ni(111) persists further away from the surface.

Finally, the energy and spin dependence of α has been calculated since it affects the apparent Ni–h-BN step height difference in a STM topograph. The spin-resolved calculations give a hint at which energy the magnetic contrast is largest, i.e., at which tip-sample voltages the largest Ni–h-BN step height differences are expected for parallel and antiparallel sample-tip spin configurations. Figure 8 shows α for the average charge (and spin) densities $|\Psi_\nu|^2(E-E_F, r_0)$ of Ni(111) and h-BN/Ni(111) on a plane parallel to the surface (at $r_0 = 5$ a.u. ≈ 2.5 Å) for the majority spin $\alpha_\uparrow$, the minority $\alpha_\downarrow$ spin, and the total charge α as a function of the energy relative to the Fermi level $E-E_F$. Above 1.5 eV, α decreases since $|\Psi_{h-BN}|^2$ increases due to the onset of the h-BN conduction (interface) band. The spin dependence of α emphasizes a magnetic contrast exceeding that of homonuclear steps. The spin anisotropy of α changes sign in going from the occupied states (minority dominated) to the unoccupied states (majority dominated). The zero anisotropy point, where $\alpha_\uparrow = \alpha_\downarrow$, is close to the Fermi level (10 meV). For $\alpha_\uparrow \neq \alpha_\downarrow$ and a tunneling tip with a nonzero spin polarization we expect a spin-dependent tunneling conductance. We therefore propose an experiment that will show magnetic contrast $\Delta z_m = \Delta z_{\uparrow\uparrow} - \Delta z_{\uparrow\downarrow}$ in a constant-conductance STM picture (topograph) where $\Delta z_{\uparrow\uparrow}$ ($\Delta z_{\uparrow\downarrow}$) is the spintronic contrast for a parallel (antiparallel) sample-tip spin configuration. For a magnetized STM tip with a polarization of $P = 10\%$ we expect at $E-E_F = 0.3$ eV a maximum magnetic contrast $\Delta z_m \approx P\lambda \ln(\alpha_\uparrow/\alpha_\downarrow)$ of $\approx 0.1\lambda$, a value that may be readily measured.

VII. SUMMARY AND CONCLUSIONS

In this work the six possible configurations of h-BN on Ni(111) were investigated in view of their stability. From the

total energy calculations it turns out that only in the two configurations with N on top of the topmost Ni atoms, h-BN is bound to the Ni surface while for all other configurations the h-BN is unbound. It is essential that N atoms sit on top of the Ni atoms and from the two possibilities for the B atom the fcc hollow site $(N,B) = (top,fcc)$ is energetically slightly favored. However, the energy difference is very small and GGA-type calculations might not have sufficient accuracy to give a decisive answer. The band structure for 19 layers of Ni(111)+2 layers of corrugated h-BN slabs was calculated for spin-up and spin-down electrons. The magnetism is reflected in the exchange-split Ni d bands which are partially empty for minority spins. The h-BN σ and π bands are identified and compared with the experimental photoemission dispersion plot from h-BN/Ni(111). h-BN does not contribute new bands that cross the Fermi level and is thus considered to remain an insulator. Bader's topological method was applied to determine the charge of the atoms compared to the superposition of atomic charge densities and the corresponding charge transfer in the solid. A charge of 0.59 electrons on nitrogen and -0.65 electrons on boron produce a transfer of 0.06 electrons per unit cell to the substrate which explains the observed (and calculated) work function shift of 1.8 eV (1.7 eV) between Ni(111) and h-BN/Ni(111). The magnetic moments for bulk Ni and for the two surfaces: Ni(111) and h-BN/Ni(111) were calculated, and the strong reduction of the magnetic moment of the Ni top layer is explained by a charge transfer from h-BN to Ni(111). The calculated local charge density at the Fermi energy assigns the contrast in the STM image to N and B sites, using the configuration with N on top and B in the fcc hollow site. The spin-resolved LDOS above the surface of Ni(111) and h-BN/ Ni(111) is used in order to propose spin-dependent tunneling experiments with high magnetic contrast.

[1] W. Auwärter, T.J. Kreutz, T. Greber, and J. Osterwalder, Surf. Sci. **429**, 229 (1999).

[2] W. Auwärter, M. Muntwiler, T. Greber, and J. Osterwalder, Surf. Sci. **511**, 379 (2002).

[3] A. Nagashima, N. Tejima, Y. Gamou, M. Terai, and C. Oshima, Phys. Rev. B **51**, 4606 (1995).

[4] Y. Gamou, M. Terai, A. Nagashima, and C. Oshima, Sci. Rep. Res. Inst. Tohoku Univ. A **44**, 211 (1997).

[5] M. Muntwiler, W. Auwärter, F. Baumberger, M. Hoesch, T. Greber, and J. Osterwalder, Surf. Sci. **472**, 125 (2001).

[6] J. Tersoff and D.R. Hamann, Phys. Rev. B **31**, 805 (1985).

[7] E. Sjöstedt, L. Nordström, and D.J. Singh, Solid State Commun. **114**, 15 (2000).

[8] G.K.H. Madsen, P. Blaha, K. Schwarz, E. Sjöstedt, and L. Nordström, Phys. Rev. B **64**, 195134 (2001).

[9] P. Blaha, K. Schwarz, G. K. H. Madsen, D. Kvasnicka, and J. Luitz, computer code WIEN2k, an augmented plane wave plus local orbitals program for calculating crystal properties, Vienna University of Technology, Vienna, 2001.

[10] K. Schwarz, P. Blaha, and G.K.H. Madsen, Comput. Phys. Commun. **147**, 71 (2002).

[11] J.P. Perdew, S. Burke, and M. Ernzerhof, Phys. Rev. Lett. **77**, 3865 (1996).

[12] P. Blöchl, O. Jepsen, and O.K. Andersen, Phys. Rev. B **49**, 16 223 (1994).

[13] G. Nicolay, F. Reinert, S. Hüfner, and P. Blaha, Phys. Rev. B **65**, 033407 (2001).

[14] T. Greber, O. Raetzo, T.J. Kreutz, P. Schwaller, W. Deichmann, E. Wetli, and J. Osterwalder, Rev. Sci. Instrum. **68**, 4549 (1997).

[15] A. Nagashima, N. Tejima, Y. Gamou, T. Kawai, and C. Oshima, Phys. Rev. Lett. **75**, 3918 (1995).

[16] C. Oshima and A. Nagashima, J. Phys.: Condens. Matter **9**, 1 (1997).

[17] E. Rokuta, Y. Hasegawa, K. Suzuki, Y. Gamou, C. Oshima, and A. Nagashima, Phys. Rev. Lett. **79**, 4609 (1997).

[18] The uncertainty of 4 meV corresponds to the residual scatter of iterations in the converged structure.

[19] A. Catellani, M. Posternak, A. Baldereschi, and A.J. Freeman, Phys. Rev. B **36**, 6105 (1987).

[20] T. Greber, W. Auwärter, M. Hoesch, G. Grad, P. Blaha, and J. Osterwalder, Surf. Rev. Lett. **9**, 1243 (2002).

[21] R. F. W. Bader, *Atoms in Molecules—A Quantum Theory* (Oxford University Press, Oxford, 1990).

[22] C.L. Fu and A.J. Freeman, J. Phys. (Paris), Colloq. **49**, C8-1625 (1988).

[23] J. Tersoff and L.M. Falicov, Phys. Rev. B **26**, 6186 (1982).

[24] T. Greber, W. Auwätrter, G. Grad, P. Blaha, and J. Osterwalder, in *Proceedings of the Third International Symposium on Atomic Level Characterization for New Materials and Devices ALC'01, Nara, Japan, 2001* (unpublished).

[25] J. Bardeen, Phys. Rev. Lett. **6**, 57 (1961).

[26] P. Sautet, Chem. Rev. (Washington, D.C.) **97**, 1097 (1997).